Doughnut-shaped structure of a bacterial muramidase revealed by X-ray crystallography

Thunnissen, Andy; Dijkstra, Arnoud J.; Kalk, Kor H.; Rozeboom, Henriette; Engel, Henk; Keck, Wolfgang; Dijkstra, Bauke W.

Published in:
Nature

DOI:
10.1038/367750a0

entially activated in the cytosol and nucleus. We propose that such enzymes will be activated in the cytosol by brief cytosolic Ca^{2+} transients, but will remain largely inactive in the nucleus, where the Ca^{2+} change is attenuated. Such enzymes will be activated in the nucleus only after a long-lived cytosolic Ca^{2+} change. The pattern of calmodulin activation in neurons is consistent with this scheme: brief depolarization activates cytosolic calmodulin[21], but calmodulin-dependent transcription of the c-*fos* gene[1] occurs only after intense synaptic stimulation or pathological cell depolarization[22,23]. □

Received 14 September; accepted 29 December 1993.

1. Sheng, M., McFadden, G. & Greenberg, M. E. *Neuron* **4,** 571–582 (1990).
2. Bachs, O., Agell, N. & Carafoli, E. *Biochim. biophys. Acta.* **1113,** 259–270 (1992).
3. Murdoch, G. H., Waterman, M., Evans, R. M. & Rosenfeld, M. G. *J. biol. Chem.* **260,** 11852–11858 (1985).
4. Graham, R. & Gilman, M. *Science* **251,** 189–192 (1991).
5. Mehmet, H. & Rozengurt, E. *B. med. Bull.* **47,** 76–86 (1991).
6. Paine, P. L., Moore, L. C. & Horowitz, S. B. *Nature* **254,** 109–114 (1975).
7. Hinshaw, J. E., Carragher, B. O. & Milligan, R. A. *Cell* **69,** 1133–1141 (1992).
8. Williams, D. A., Fogarty, K. E., Tsien, R. Y. & Fay, F. S. *Nature* **318,** 558–561 (1985).
9. Neylon, C. B., Hoyland, J., Mason, W. T. & Irvine, R. F. *Am. J. Physiol.* **259,** C675–C686 (1990).
10. Waybill, M. M. *et al. Am. J. Physiol.* **261,** E49–E57 (1991).
11. Himpens, B., DeSmedt, H., Droogmans, G. & Casteels, R. *Am. J. Physiol.* **263,** C95–C105 (1992).
12. Wahl, M., Sleight, R. G. & Gruenstein, E. *J. cell. Physiol.* **150,** 593–609 (1992).
13. Hernandez-Cruz, A., Sala, F. & Adams, P. R. *Science* **247,** 858–862 (1990).
14. Holliday, J., Adams, R. J., Sejnowski, T. J. & Spitzer, N. C. *Neuron* **7,** 787–796 (1991).
15. Birch, B. D., Eng, D. L. & Kocsis, J. D. *Proc. natn. Acad. Sci. U.S.A.* **89,** 7978–7982 (1992).
16. Stricker, S. A., Centonzee, V. E., Paddick, S. W. & Schatten, G. *Devl Biol.* **149,** 370–380 (1992).
17. Minta, A., Kao, J. P. Y. & Tsien, R. Y. *J. biol. Chem.* **264,** 8171–8178 (1989).
18. Connor, J. A. *Cell Calcium* **14,** 185–200 (1993).
19. Forbes, D. J. *A. Rev. Cell Biol.* **8,** 495–527 (1992).
20. DiVirgilio, F., Steinberg, T. H. & Silverstein, S. C. *Cell Calcium* **11,** 57–62 (1990).
21. Chad, J. E. & Eckert, R. *J. Physiol., Lond.* **378,** 31–51 (1986).
22. Dragunow, M. *et al. Neurosci. Lett.* **101,** 274–280 (1989).
23. Morgan, J. I., Cohen, J. L., Hempstead, J. L. & Curran, T. *Science* **237,** 192–197 (1987).
24. Silver, R. A., Lamb, A. G. & Bolsover, S. R. *Nature* **343,** 751–754 (1990).
25. Al-Mohanna, F. A., Cave, J. & Bolsover, S. R. *Dev. Brain Res.* **70,** 287–290 (1992).

ACKNOWLEDGEMENTS. We thank M. Nirenberg for the N1E-115 cells and M. Duchen, D. Attwell, A. Silver, L. Bindman and M. Whitaker for their help. This work was supported by the Wellcome Trust and the MRC.

Doughnut-shaped structure of a bacterial muramidase revealed by X-ray crystallography

Andy-Mark W. H. Thunnissen*, Arnoud J. Dijkstra†, Kor H. Kalk*, Henriëtte J. Rozeboom*, Henk Engel*‡, Wolfgang Keck† & Bauke W. Dijkstra*§

* BIOSON Research Institute, Department of Chemistry, University of Groningen, Nijenborgh 4, 9747 AG Groningen, The Netherlands
† F. Hoffmann-La Roche Ltd, Pharma Research Department, CH-4002 Basel, Switzerland

THE integrity of the bacterial cell wall depends on the balanced action of several peptidoglycan (murein) synthesizing and degrading enzymes[1,2]. Penicillin inhibits the enzymes responsible for peptide crosslinks in the peptidoglycan polymer[3]. Enzymes that act solely on the glycosidic bonds are insensitive to this antibiotic, thus offering a target for the design of antibiotics distinct from the β-lactams. Here we report the X-ray structure of the periplasmic soluble lytic transglycosylase (SLT; M_r 70,000) from *Escherichia coli*. This unique bacterial exomuramidase cleaves the β-1,4-glycosidic bonds of peptidoglycan to produce small 1,6-anhydromuropeptides[4–6]. The structure of SLT reveals a 'superhelical' ring of α-helices with a separate domain on top which resembles the fold of lysozyme. Site-directed mutagenesis and a crystallographic inhibitor-binding study confirmed that the lysozyme-like domain contains the active site of SLT.

Details of the structure determination are shown in Table 1. The unusually shaped SLT molecule is built up of three domains, which are all very rich in α-helices (Fig. 1). In total, about 63% of all amino-acid residues are in α-helices, the remaining residues being mostly in the helix-connecting turns and loops. The N-terminal domain (residues 1–360) contains 22 α-helices packed in an extended, U-shaped conformation. This U-domain is connected by a long loop of ~20 residues to a small linker domain (residues 381–450) of four α-helices. Together these first two domains form a closed ring with a large central hole (Fig. 1*a*, *c*). The C-terminal domain (C-domain; residues 451–618) is packed on top of this ring (Fig. 1*b*), interacting with part of the linker domain and the C-terminal region of the U-domain. It has a globular structure, containing nine α-helices, but also includes a very irregular sheet of three small antiparallel β-strands. Overall, the SLT molecule can be described as an asymmetrically shaped doughnut with dimensions of ~85 × 75 × 55 Å. The central hole has a diameter varying from 25 to 35 Å.

The α-helices in the ring-shaped U and linker domains form a double-layered right-handed superhelix. Helices in either layer of this superhelix run parallel to each other, but antiparallel to the helices of the other layer (Fig. 1*c*). The exception is helix H12, which is inserted as an antiparallel helix in the outer layer, permitting the curve in the U-domain. The helix-to-helix packing in the first two domains of SLT is distinct from that observed in four-α-helix bundles, for which structurally adjacent helix pairs are all antiparallel[7]. This superhelix of helices is not unique, however, having first been observed in the crystal structure of the lipovitellin–phosvitin complex from lamprey yolk[8]. Stabilization is provided by the burying of hydrophobic residues at the helical interfaces and by specific main chain–side chain and side chain–side chain interactions between residues of adjacent helices (Fig. 1*d*). There is a disulphide bridge between residues 106 and 139 connecting helices H7 and H9. In addition, proline residues are probably important for tightening of the U-domain, especially in the first half where nearly every helix-connecting loop contains one or two of these residues. One proline residue is located in the middle of helix H15, which shows a pronounced kink. Similar kinks in α-helices, caused by internal prolines, have been noted in a number of other proteins[9,10].

The C-domain of SLT resembles the fold of lysozyme. Figure 2*a* and *b* shows a superposition of the C-domain of SLT on hen egg-white lysozyme[11] (HEWL) and lysozyme from bacteriophage T4 (T4L; ref. 12). The structural similarity is remarkable in view of the absence of any significant sequence homology. We showed that the active site of SLT is located in the C-domain by difference Fourier analysis of an SLT–inhibitor complex at 3.5 Å resolution (Fig. 3*b*, *c*). Although a more detailed analysis of the SLT–inhibitor complex awaits data at higher resolution, preliminary results confirm the similarity with the lysozymes. The glucosaminyl part of the inhibitor is bound at a position similar to subsite C in the active sites of HEWL and T4L, whereas the proline part is bound close to Glu 478 occupying a region analogous to subsite D in the lysozymes. Glu 478 in SLT most probably functions as the 'catalytic' acid. In the structure alignment it coincides with both the 'catalytic' glutamic acid of HEWL (Glu 35) and that of T4L (Glu 11). Moreover, mutation of this residue to a glutamine gave a completely inactive enzyme,

‡ Present address: University Hospital Rotterdam-Dijkzigt, Department of Clinical Chemistry, Dr. Molewaterplein 40, 3015 GD Rotterdam, The Netherlands.
§ To whom correspondence should be addressed.

in line with a role as protein donor in a lysozyme-like reaction mechanism[13]. In contrast, there is no residue in the β-sheet of SLT that could take up the role of the catalytic aspartate of the lysozymes. Instead, coming from the upper lobe of the C-domain, the carboxylate from Glu 583 is close to the presumed reaction centre (Fig. 2). Its negative charge is, however, not critical, as a E583Q (Glu → Gln) mutant still has considerable catalytic activity. But it may be argued that there should be no strict requirement for a second carboxylate group in the catalytic mechanism of SLT. In SLT the intramolecular C6-hydroxyl group of saccharide D, rather than a water molecule, appears to be the nucleophile that attacks the C1 carbon of a possible

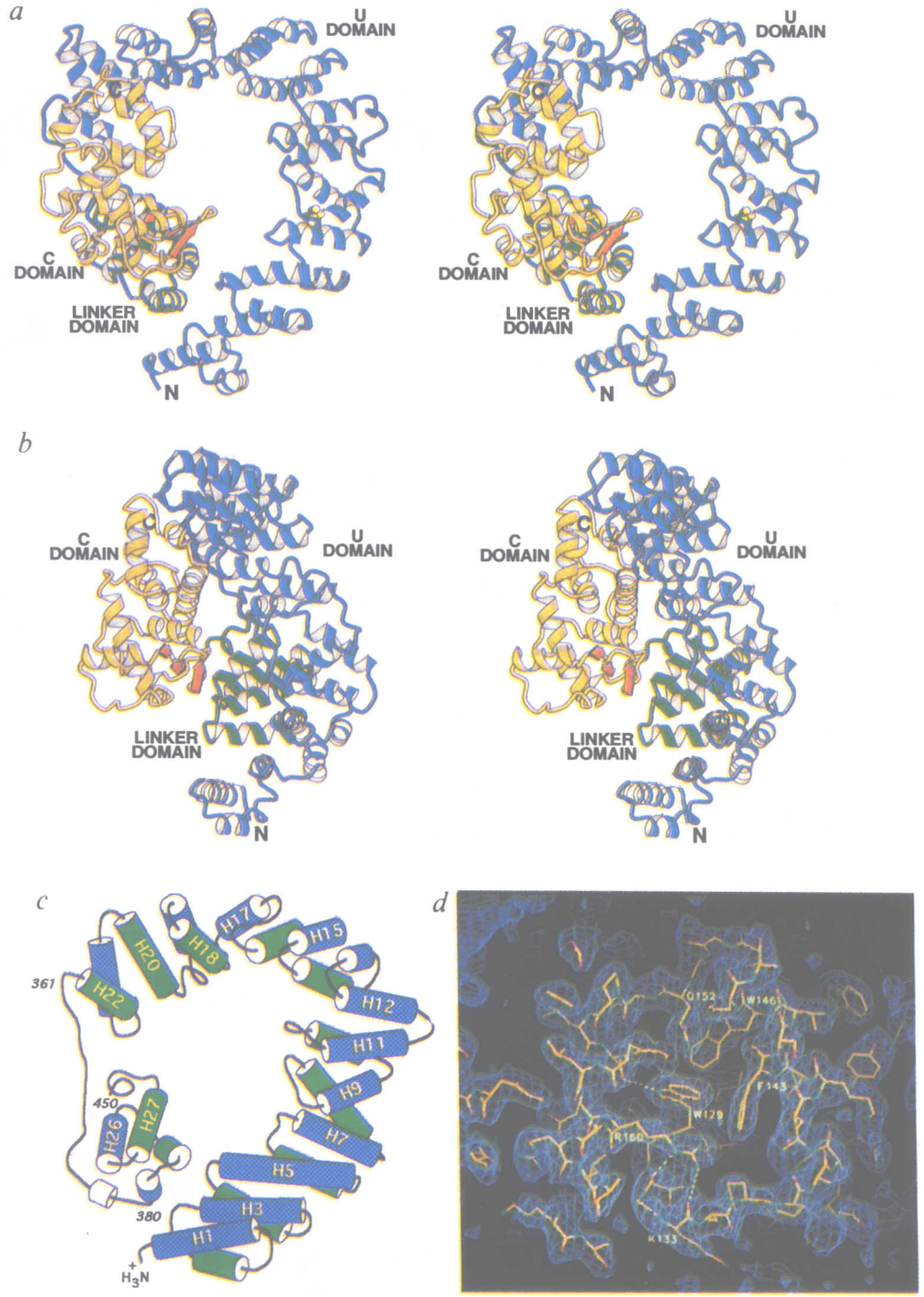

FIG. 1 *a*, A ribbon stereo representation of the model of SLT generated using the program MOLSCRIPT[24]. The colour assignment is as follows: blue, the N-terminal or U-domain; green, the linker domain; yellow, the C-terminal or C-domain. The N terminus of the polypeptide chain is located at the lower end of the U-domain. The C terminus is located at the top part of the C-domain near the U–C domain interface. Also shown are the atoms of the single disulphide bridge in SLT formed by residues 106 and 139 in helices H7 and H9 of the U-domain. *b*, Edgewise view of the SLT doughnut, showing the C-domain located on top of the helical ring. The active site of SLT is located in the groove of the C-domain flanked by the three-stranded β-sheet. *c*, Schematic representation of the U and linker domains of SLT illustrating the double-layered 'super-helical' packing of the α-helices. The two layers are identified by different colours of the helices. Residues 361 to 380 form an extended interdomain loop that is wrapped around part of the C-domain in the complete SLT molecule. *d*, A 2.7 Å ($2F_o - F_c$) electron density map calculated with refined model phases and contoured at 1σ, displaying part of the interface of helices H8, H9 and H10 (residues 129 to 165). Possible hydrogen-bond contacts between side-chain and main-chain atoms are indicated by dashed lines.

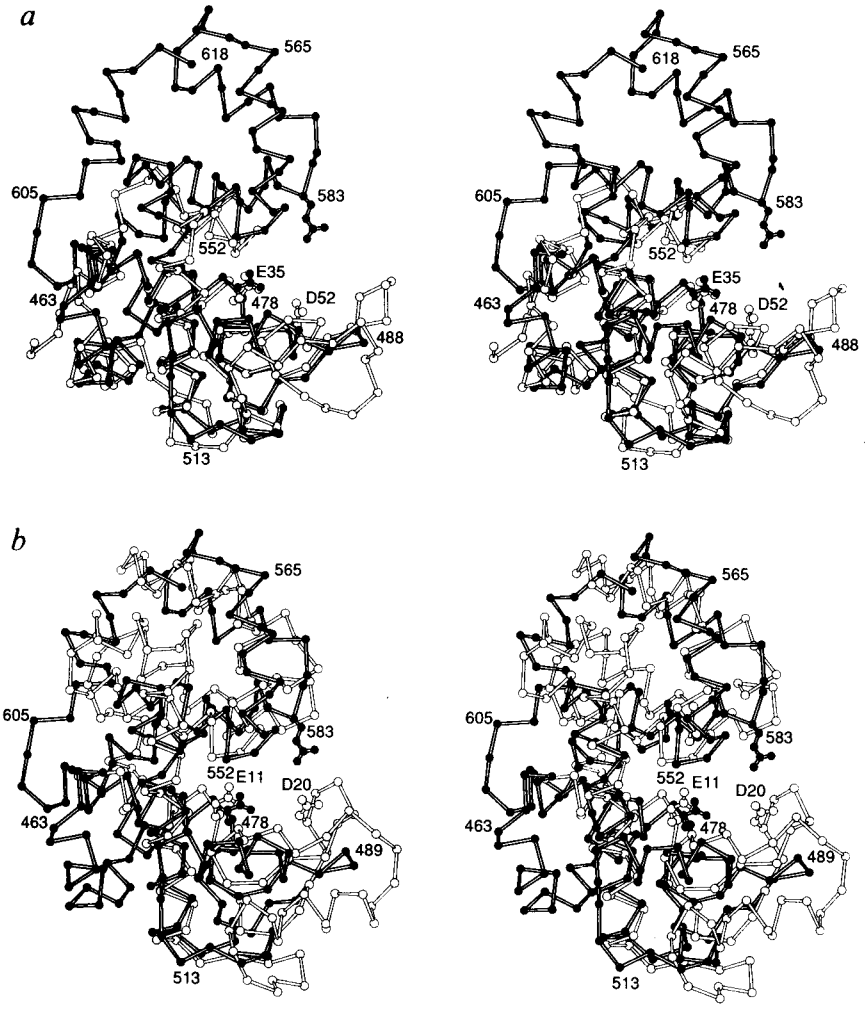

FIG. 2 Backbone comparison of the C-domain of SLT with lysozyme from hen egg-white (*a*) and lysozyme from bacteriophage T4 (*b*) using the Rossmann–Argos alignment method[25]. The α-carbon backbone of the C-domain of SLT is represented by dark solid spheres connected by thick lines, the backbone of the lysozymes by open spheres and thin lines. Residue numbers refer to the SLT sequence. The overall structure of the C-domain clearly shows most of the features common to the lysozyme fold: it is ellipsoidal in shape with two lobes linked by a long α-helix. A deep groove separates the two lobes. The lower N-terminal lobe includes some helices and a very irregular sheet of three small, antiparallel β-strands. The upper C-terminal lobe is predominantly helical, built up of five different α-helices. Unique features of the SLT C-domain that have no counterpart in either of the two lysozymes include the region between the β-sheet and the longer linker helix, and the last regions of the C-terminal lobe. Also shown are the side chains of Glu 478 and Glu 583 in SLT (dark solid atoms) compared with those of the catalytic residues in the lysozymes (E35/D52 and E11/D20 for HEWL and T4L, respectively). Coordinates for the lysozymes were obtained from the Protein Data Bank[26].

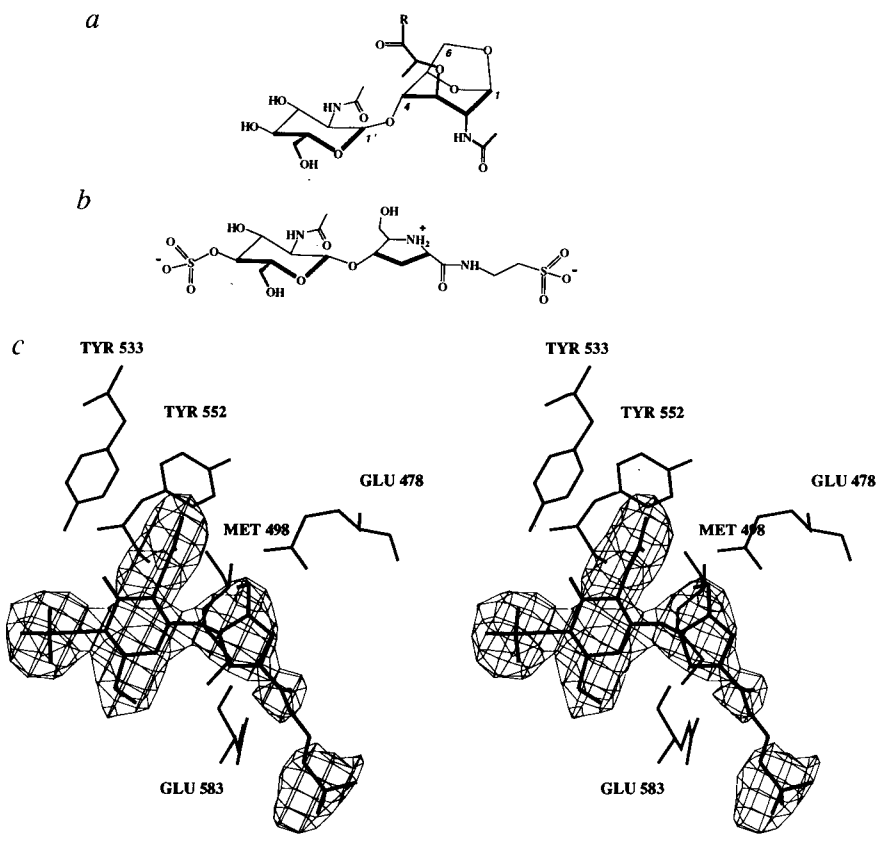

FIG. 3 *a*, Chemical structure of the muropeptide product of the reaction catalysed by SLT. The reaction product consists of a disaccharide of *N*-acetylglucosamine and *N*-acetylmuramic acid with an intramolecular anhydro-bond between C_1 and C_6. The C_3-lactyl group of the muramic acid is linked to an oligopeptide (R), consisting of L-alanine, D-glutamic acid, meso-diaminopimelic acid and D-alanine residues. The peptide may be crosslinked to that of another disaccharide forming dimeric muropeptides[5]. *b*, Structure of bulgecin A. This compound is a bacterial metabolite produced by *Pseudomonas acidophila* and *mesoacidophila*, which has bulge-inducing and lysis-enhancing activity when used in combination with β-lactam antibiotics[27]. Recently it has been found that SLT is inhibited by bulgecin A[28]. *c*, Stereographic view of a 3.5-Å $(F_o - F_c)\exp(i\alpha_c)$ difference electron density map of the SLT–bulgecin complex, contoured at 1.5σ, showing the bulgecin A inhibitor bound in the active site of SLT (F_o represents the observed structure factor amplitudes for the SLT–bulgecin complex, F_c and α_c are calculated structure factor amplitudes and phases from the refined, uncomplexed model). Residues in the active site of SLT that might interact with bulgecin A are indicated. The inhibitor was soaked into the crystals of native SLT for 2 days (7 mM inhibitor in a solution of 40% ammonium sulphate in 0.1 M sodium acetate, pH 5.0). Diffraction data to 3.3 Å resolution were collected on a FAST area detector and merged using programs of the Groningen BIOMOL crystallographic package (R_{merge} = 8.1%).

TABLE 1 Data collection and phasing statistics

	Native-I	Native-II	$KAuCl_4$-I	$KAuCl_4$-II	Pt(ethylene) $(NH_3)_2Cl_2$
Data collection					
Resolution (Å)	3.1	2.7	3.1	3.0	3.1
Observations (no.)	42,639	132,289	23,051	16,287	24,639
Unique reflections (no.)	15,409	32,225	11,062	8,232	12,616
Completeness (%)	87	96	61	45	71
R_{merge}*	0.052	0.072	0.080	0.110	0.044
R_{deriv}†			0.17	0.22	0.12
Concentration of HA (mM)‡			2	2	0.5
Phasing statistics					
Resolution included (Å)			3.3	3.5	3.3
Heavy-atom sites			3	3	5
Occupancies O_r/O_a§			36.1/4.8	28.7/6.1	21.4/3.0
R_{Cullis}‖			0.57	0.69	0.62
Phasing power¶			2.2	1.0	1.9

Native SLT was prepared and crystallized as described[6,17]. The spacegroup is $P2_12_12_1$ with cell dimensions $a=80.8$ Å, $b=88.4$ Å and $c=132.1$ Å. Native and derivative data used in isomorphous replacement were measured on a FAST area detector (Enraf–Nonius, Delft, The Netherlands) connected to an Elliot GX-21 rotating anode generator, and reduced using the programs MADNES[18], XDS[19] and software of the Groningen BIOMOL package. For the $KAuCl_4$ derivative, an additional data set ($KAuCl_4$-II) was collected on the FAST system of the Brookhaven National Laboratory X12C beamline at the NSLS, Upton, NY. Native data to 2.7 Å were collected on the MAR Research image plate system at the synchrotron beamline X31 of the EMBL Outstation at DESY, Hamburg. Evaluation and reduction of these data were carried out using modified versions of the MOSCO programs (Hamburg, Germany) and programs of the CCP4 suite (Daresbury, UK). Heavy-atom parameters were refined with PHARE[20]. A map was calculated to 3.3 Å which had a mean figure-of-merit of 0.60 for 10,396 reflections between 35.0 and 3.3 Å resolution. The map was improved by solvent flattening and an initial protein model was fitted to the density using FRODO[21] and O[22]. The model was gradually improved by energy minimization using X-PLOR[23] alternated with model-building sessions in maps calculated with combined phases. A few rounds of simulated annealing refinement improved the model further. In the last stages of refinement, some water molecules were added, based on peaks in ($Fo-Fc$) difference Fourier maps higher than 3σ and requiring at least two favourable hydrogen-bonding interactions with protein atoms. The present model contains all 618 residues and 22 water molecules. No breaks in the electron density were observed at the 1σ level for the entire polypeptide backbone except at residue 371, which forms part of a long extended loop connecting the first two domains. The current R-factor for 22,643 reflections between 8.0 and 2.7 Å resolution ($F \geq 2\sigma(F)$) is 22.8% after a restrained B-factor refinement. Root-mean-square deviations from ideality in bond lengths and angles are 0.019 Å and 3.6 °, respectively.

* $R_{merge}=\sum_h\sum_i|I_{(h,i)}-\langle I\rangle_{(h)}|/\sum_h\sum_i\langle I\rangle_{(h)}$; $I_{(h,i)}$ is the scaled intensity of the ith observation of reflection h and $\langle I\rangle_{(h)}$ is the mean value.

† $R_{deriv}=\sum_h|F_{PH}-F_P|/\sum_h F_P$; F_{PH} and F_P are the structure factor amplitudes for native and derivative data.

‡ For data collection and soaking experiments involving heavy atoms (HAs), crystals of SLT were transferred to a stabilizing solution of 40% saturated ammonium sulphate in 0.1 M sodium acetate buffer, pH 5.0.

§ O_r and O_a represent real and anomalous occupancy of the strongest heavy-atom site in arbitrary units, proportional to the number of electrons.

‖ $R_{Cullis}=\sum_h||F_{PH,obs}\pm F_{P,obs}|-F_{H,calc}|/\sum_h|F_{PH,obs}\pm F_{P,obs}|$; for centric reflections only.

¶ Phasing power $=[\sum_h|F_{H,calc}|^2/\sum_h(|F_{PH,obs}|-|F_{PH,calc}|)^2]^{1/2}$.

oxocarbonium intermediate (Fig. 3*a*). Such an intramolecular attack would probably require a shorter lifetime of the oxocarbonium intermediate, and thus less stabilization, as the reaction is no longer dependent on the diffusion-controlled replacement of the leaving group with a water molecule[14,15].

The crystal structure of SLT will be used for the design of specific inhibitors that might form a basis for the development of novel types of antibiotics. Meanwhile, further research is needed to obtain more information about the mechanism of peptidoglycan binding and cleavage. Most intriguing is the question of the function of the U and linker domains. They might be needed to enhance substrate affinity by providing additional murein-binding sites. In addition, the central hole could impose exo-enzymatic activity[16] upon the lysozyme-like C-domain: indeed, the active-site groove in the C-domain is oriented in such a way that a glycan strand bound with its GlcNAc end towards site A would run with its other end through the central hole, close to the surface of the linker domain. □

Received 29 September; accepted 13 December 1993.

1. Rogers, H. J., Perkins, H. R. & Ward, J. B. in *Microbial Cell Walls and Membranes* (eds Perkins, H. R. *et al.*) 437–460 (Chapman & Hall, London, 1980).
2. Höltje, J.-V. & Schwarz, U. in *Molecular Cytology of* Escherichia coli (ed. Nanninga, N.) 77–119 (Academic, London, 1985).
3. Waxman, D. J. & Strominger, J. L. *A. Rev. Biochem.* **52,** 825–869 (1983).
4. Höltje, J.-V., Mirelman, D., Sharon, N. & Schwarz, U. *J. Bact.* **124,** 1067–1076 (1975).
5. Keck, W., Wientjes, F. B. & Schwarz, U. *Eur. J. Biochem.* **148,** 493–497 (1985).
6. Engel, H., Kazemier, B. & Keck, W. *J. Bact.* **173,** 6773–6782 (1991).
7. Presnell, S. R. & Cohen, F. E. *Proc. natn. Acad. Sci. U.S.A.* **86,** 6592–6595 (1989).
8. Banaszak, L., Sharrock, W. & Timmins, P. A. *Rev. Biophys. biophys. Chem.* **20,** 221–246 (1991).
9. Barlow, D. J. & Thornton, J. M. *J. molec. Biol.* **201,** 601–619 (1988).
10. Verschueren, K. H. G., Franken, S. M., Rozeboom, H. J., Kalk, K. H. & Dijkstra, B. W. *J. molec. Biol.* **232,** 856–872 (1993).
11. Imoto, T., Johnson, L. N., North, A. C. T., Phillips, D. C. & Rupley, J. A. in *The Enzymes* (ed. Boyer, P. D.) 666–868 (Academic, New York, 1972).
12. Weaver, L. H. & Matthews, B. W. *J. molec. Biol.* **193,** 189–199 (1987).
13. Blake, C. C. F. *et al. Proc. R. Soc. Lond.* B**167,** 378–388 (1967).
14. Hardy, L. W. & Poteete, A. R. *Biochemistry* **30,** 9457–9463 (1991).
15. Strynadka, N. C. J. & James, M. N. G. *J. molec. Biol.* **220,** 440–424 (1991).
16. Beachey, E. H., Keck, W., de Pedro, M. A. & Schwarz, U. *Eur. J. Biochem.* **116,** 355–358 (1981).
17. Rozeboom, H. J., Dijkstra, B. W., Engel, H. & Keck, W. *J. molec. Biol.* **212,** 557–559 (1990).
18. Messerschmidt, A. & Pflugrath, J. W. *J. appl. Crystallogr.* **20,** 306–315 (1987).
19. Kabsch, W. *J. appl. Crystallogr.* **21,** 916–924 (1988).
20. Bricogne, G. *Acta crystallogr. A* **32,** 832–847 (1976).
21. Jones, T. A. *J. appl. Crystallogr.* **11,** 268–272 (1978).
22. Jones, T. A., Zou, J.-Y., Cowan, S. W. & Kjeldgaard, M. *Acta crystallogr.* A**47,** 110–119 (1991).
23. Brünger, A. T. *X-PLOR (Version 3.0) Manual* (Yale Univ., New Haven, 1992).
24. Kraulis, P. J. *J. appl. Crystallogr.* **24,** 946–950 (1991).
25. Rossmann, M. G. & Argos, P. *J. molec. Biol.* **105,** 75–96 (1976).
26. Bernstein, F. C. *et al. J. molec. Biol.* **112,** 535–542 (1977).
27. Shinagawa, S., Maki, M., Kintaka, K., Imada, A. & Asai, M. *J. Antibiot.* **38,** 17–23 (1985).
28. Templin, M. F., Edwards, D. H. & Höltje, J.-V. *J. biol. Chem.* **267,** 20039–20043 (1992).

ACKNOWLEDGEMENTS. We thank K. Wilson and R. M. Sweet for data collection facilities at EMBL-DESY and BNL-NSLS, and L. Banaszak for the Cα coordinates of the helical domain of the lipovitellin structure. Bulgecin A was obtained from Takeda Chemical Industries Ltd, Osaka. This research was supported by the Netherlands Foundation for Chemical Research and the Netherlands Organisation for Scientific Research.